Journal of
Materials Chemistry B

Materials for biology and medicine

Accepted Manuscript

This is an Accepted Manuscript, which has been through the Royal Society of Chemistry peer review process and has been accepted for publication.

Accepted Manuscripts are published online shortly after acceptance, before technical editing, formatting and proof reading. Using this free service, authors can make their results available to the community, in citable form, before we publish the edited article. We will replace this Accepted Manuscript with the edited and formatted Advance Article as soon as it is available.

You can find more information about Accepted Manuscripts in the Information for Authors.

Please note that technical editing may introduce minor changes to the text and/or graphics, which may alter content. The journal's standard Terms & Conditions and the Ethical guidelines still apply. In no event shall the Royal Society of Chemistry be held responsible for any errors or omissions in this Accepted Manuscript or any consequences arising from the use of any information it contains.

ROYAL SOCIETY OF CHEMISTRY

rsc.li/materials-b

Shape Memory Histocompatible and Biodegradable Sponges for Subcutaneous Defect Filling and Repair: Greatly Reducing Surgical Incision

Yanteng Zhao[1,2], Yinping Li[1], Qiaoyue Du[1], Qiang Zhang[1], Xianping Lv[2], Qiankun Yang[2], Peter R. Chang[4], Debbie P. Anderson[4], Meng He[3*] and Yun Chen[1*]

[1]*Department of Biomedical Engineering, School of Basic Medical Sciences, Wuhan University, Wuhan 430071, China*

[2]*Department of Transfusion, The First Affiliated Hospital of Zhengzhou University, Zhengzhou 450052, China*

[3]*School of Materials Science and Engineering, Yancheng Institute of Technology, Yancheng, Jiangsu 224051, China*

[4]*Bioproducts and Bioprocesses National Science Program, Agriculture and Agri-Food Canada, 107 Science Place, Saskatoon, SK, S7N 0X2, Canada*

*Corresponding author. Tel.: +86 27 6875 9509; fax: +86 27 6875 9142. *E-mail address:* yunchen@whu.edu.cn (Yun Chen), hemeng315@163.com (Meng He).

Abstract

Reducing surgical incision for large area subcutaneous defect filling and repair is a great challenge in the biomedical field especially for plastic surgery. In this study, novel hydroxyethyl cellulose/soy protein isolate (HEC/SPI) composite sponges (EHSS) with fluid responsive shape memory property were constructed, whose thickness could be controlled by hot-pressing conditions to reduce the required surgical incision greatly. Effects of the main factors such as pressure, temperature and hot-pressing cycles on the recovery degree of EHSS were investigated systematically. The structure and physical properties of the sponges were characterized by FTIR, XRD and SEM etc. The results showed that EHSS could be pressed into thin disks with much smaller thickness, and the thickness retention ratio and recovery ratio were affected by hot-pressing conditions such as pressure and temperature. Especially, EHSS could be hot-pressed into a dense thin disk (EHSS-PT-130) at 130 ^{o}C with the pressure of 30 MPa, which could quickly recover its original shape by soaking in hydrophilic fluids. EHSS-PT-130 also exhibited good hydrophilicity, cytocompatibility, histocompatibility and *in vivo* biodegradability. Compared with original EHSS, *in vivo* shape memory EHSS-PT-130 required much smaller surgical incision to reach the same repair effect and no need of extra sterilization, showing potential application for subcutaneous defect filling and repair.

Key words: hydroxyethyl cellulose, soy protein isolate, shape memory, histocompatibility, subcutaneous filling and repair

1. Introduction

Soft tissues can be subdivided into five types: epithelial, connective, parenchymal, muscle, and nerve tissue, which include skin, adipose tissue and ligament etc[1-3]. Soft tissue defect usually occurs because of age or injury, resulting in the reduction of its functions in connecting, supporting, and protecting other body structure. Moreover, the concave deformity caused by soft tissue defect will affect the appearance and even activity function of patients, which will further affect their psychological health and life quality. In 2019, the worldwide market requirement for soft tissue repair is expected to reach 14.7 billion US dollars[4]. Thus, the repair of clinically soft tissue defect and the surgical reconstruction of soft tissue is one of the main problems of plastic surgery. At present, the main methods for tissue defect repair include autologous transplantation[5,6], allograft transplantation and filling of artificial materials[7-10]. Autograft and allograft transplantations could create new wounds and scars, and the implanted tissue is usually unstable and couldn't satisfy the purpose of filling and possibly cause secondary deformities. Furthermore, the allograft tissue transplants exhibit other problems such as immune inhibition. Therefore, artificial filling materials would become the most promising soft tissue repair materials in the future[11]. At present, the commonly used artificial filling materials mainly include poly methyl-methacrylate[12-13], methacrylate hydrogels[14], silica gel[7,8,15] and PTFE[16,17] etc. However, some of these implanted materials couldn't be degraded in the body that will restrict their application as soft tissue repair, other implanted materials exhibit poor biocompatibility and cannot combine with tissues tightly. Injectable gels could also be used for soft tissue repair, but their mechanical strength is usually weak[18]. So the development of novel biocompatible, safe, effective, and degradable filling materials in vivo has become a hotspot and challenge for plastic surgery.

Ideal soft tissue biomaterials need to be pliable to match the contours of tissue defect, while offer adequate mechanical support to prevent defect collapse [19]. These systems also require interconnected pores of about 100−300 μm to allow the exchange of gases and nutrients, the infiltration of cells for tissue ingrowth and vascularization, as well as degradation rates that could match the kinetics of de novo tissue formation[20-22,23].

Biopolymer-based sponges have extraordinary advantages such as biodegradability, safe and good biocompatibility[24]. As far as we know, several biopolymer-based sponges such as silk protein have been used successfully for soft tissue engineering[19,25]. However, large area defects usually require large blocks of sponges, so a large surgical incision was usually inevitable, which would leave a large scar after operation correspondingly. Interestingly, some sponges could become shrunk after being compressed, and the sponge volume would become much smaller correspondingly due to the existence of abundant pores[26,27]. It was noted that water reversible cubic scaffolds from nanocellulose and nanochitin were fabricated for biomimetic tissue engineering, which shrank obviously after drying but recovered their original shape after water soaking[28]. Thus, a worthwhile endeavor would be to create a shape-memory sponge for soft tissue defect repair that could shrink after being compressed while recover its original shape after being in vivo implanted in body fluid-containing environment.

In our previous work, biocompatible, hemocompatible and biodegradable hydroxyethyl cellulose/soy protein isolate (HEC/SPI) composite films were fabricated[29], which had wide potential application as biomaterials. In this work, HEC and SPI were also used as raw materials to construct shape-memory sponges with macro-pores structure that could be hot-pressed into a thin disk, but could almost recover their original size quickly after soaking in hydrophilic fluids. The effects of the main factors such as pressure, temperature, hot-pressing and its cycles on the recovery degree of the sponges were investigated systematically. The result of subcutaneous filling and repair experiment in rats showed that the required surgical incision for the hot-pressed sponge was much smaller but had the feasibility of quick shape-recovery *in vivo*, which exhibited the same good filling and repair function for soft tissue defect, showing wide application in the biomedical field.

2. Materials and methods

2.1 Materials

Hydroxyethyl cellulose (HEC, with viscosity of 30000 mPa) was purchased from Shandong Head Reagent Co. Ltd. (Shandong, China). Commercial soy protein isolate (SPI)

was obtained from DuPont-Zhengzhou Protein (Zhengzhou, China). HEC and SPI were vacuum-dried for 24 h at 60 ºC before use. Epichlorohydrin (ECH) (analytical grade, liquid, 1.18 g/mL). Modified Eagle's Medium (MEM), fetal bovine serum (FBS) and 3-[4,5-dimethyl-2- thiazoly1]-2,5-diphenyl-2H-tetrazolium bromide (MTT) were obtained from Invitrogen Corporation (Gibco BRL, Grand Island, NY, USA). Other chemicals were analytical grade and used without further treatment.

2.2 Construction of sponges and sponge sheets from different hot-pressing treatments

ECH-crosslinked HEC/SPI sponges (EHSS) were prepared by crosslinking HEC/SPI blend solutions (the dry weight ratio of 3:7) with ECH and the following freeze-drying process. The details are provided in the Supplementary Material. The dried EHSS sponges were cut into blocks with required size, and treated by different temperature and pressure controlled by a thermo-compressor. All these samples after being pressed, heated or hot-pressed were called as "Treat EHSS" and the Treated EHSS were divided into four groups. The treatment process for each group and corresponding sample codes are shown in Scheme 1, and the details for each group are shown in the Supplementary Material. Treated EHSS were soaked in water for 24 h and then freezing-dried. These resulted sponges were coded as "Recovered EHSS". Effects of treatment process on the differences among original EHSS, Treated EHSS and Recovered EHSS were compared for the investigation of the shape memory property of EHSS.

2.3 Characterization

The structure and thermal properties of the EHSS were characterized by attenuated total reflectance Fourier transform infrared spectroscope (ATR-FTIR), X-ray diffractometer (XRD), scanning electron microscope (SEM) and thermogravimetric (TG). The corresponding details in methods are provided in the Supplementary Material. The original height (thickness) of the composite sponges was abbreviated as H_o, H_t and H_r corresponded to the thicknesses of treated EHSS and recovered EHSS, respectively. The thickness retention ratio after treatment and recovery ratio after water soaking and freeze-drying, namely thickness percentage ratios of treated EHSS and recovered EHSS to original EHSS, respectively, were calculated according to equation (1) and (2).

$$\text{Thickness retention ratio (\%)} = [H_t/H_o] \times 100 \quad (1)$$

$$\text{Recovery ratio (\%)} = [H_r/H_o] \times 100 \quad (2)$$

To measure the water absorption ratio, EHSS was cut into blocks (3 × 3 cm) or the Treated EHSS were dried in a vacuum oven at 60 °C for 6 h, and then weighed to determine the initial dry mass (M_1). The sponge samples were soaked in the ultrapure water for 24 h at room temperature, and then carefully wiped with filter paper to remove the excess water from the surface and weighed again (M_2). The water uptake ratio (Wu_1) was calculated according to equation (3)[30].

View Article Online

$$Wu_1(\%) = [(M_2 - M_1)/M_1] \times 100 \quad (3)$$

The relative water uptake ratio was calculated by the values of Wu_1 of Treated EHSS to that of EHSS. The swelling kinetics of EHSS and EHSS-PT-130 were also evaluated. The EHSS and EHSS-PT-130 were weighed to determine initial dry masses of (M_0), and then soaked in ultrapure water for different time intervals and weighed (M_t), and the relative water uptake ratio (Wu_2) was calculated according to equation (4).

$$Wu_2(\%) = [(M_t - M_0=)/M_0] \times 100 \quad (4)$$

The relative water uptake ratio was calculated by the values of Wu_2 of EHSS and EHSS-PT-130 to that of EHSS at equilibrium swelling state.

2.4 The sterilization efficiency of the hot-pressing treatment

The sponge disks with the diameter of 1 cm were kept in a desiccator without sterilization treatment, which were then kept between two steel molds for hot-pressing treatment with the pressure of 30 MPa and temperature of 30, 90, 130, 170 and 210 ºC, respectively. The resultant sponges were put into the Luria-Bertani solid culture plates directly and cultured for 72 h. The sterilization efficiency by different hot-pressing processes at different temperature was evaluated according to the appearance of bacterial colonies on the plate surfaces by detecting the changes in color and shape of the bottom and around the EHSS-PT-n sponges.

2.5 Cytocompatibility evaluation by MTT assay and direct culture method

The cell viability of the EHSS and all the hot-pressed sponges was evaluated by MTT assay according to our previous work[29], and the experimental details are also provided in the

Supplementary Material. The EHSS-PT-n (n = 30, 90, 130 and 210) sponges were cultured with GFP-transfected L929 cells, and the experimental details are provided in the Supplementary Material. The cells cultured on the 24 well plates without sponge samples from the same process were used as negative control. The sponges with GFP-transfected L929 cells and the negative control cells were then observed and photographed using a confocal microscope (Leica-LCS-SP8-STED, Leica, Germany). Meanwhile, the sponges with GFP-transfected L929 cells were dehydrated by immersing in 50, 70, 80, 90 and 100% (v/v) ethanol solution in sequence, frozen in liquid nitrogen, vacuum-dried, and coated with gold for SEM observation.

2.6 In vitro degradation of EHSS, subcutaneous filling and repair function evaluation of the EHSS and EHSS-PT-130

The in vitro degradation behavior of EHSS was studied, and the experimental details are provided in the Supplementary Material. The subcutaneous filling and repair function of EHSS and EHSS-PT-130 were evaluated according to the standard of ISO 10993-6. Thirty Sprague−Dawley (SD) female rats, weighing 200-250 g, were obtained from the Wuhan University Laboratory Animal Center (WHULAC, China) and acclimatized in the animal care facility for 2 weeks prior to surgery. These rats were randomly divided into two groups (15 rats per group). EHSS blocks (diameter of 10 mm, thickness of 3.40 mm, sterilized by high pressure steam) and EHSS-PT-130 thin disks (diameter of 10 mm, thickness of 0.14 mm, no autoclave sterilization needed because of the same sterilization efficiency of hot-pressing) were used as incision filling materials for EHSS and EHSS-PT-130 groups, respectively.

The rats were anaesthetized by intraperitoneal injection of 7 wt% chloral hydrate with the amount of 1 mL/200 g. After anesthesia, the operation area was disinfected with iodine and 75% alcohol, two incisions were cut on both sides along the spine of the back. EHSS-PT-130 was implanted in the left side incisions and EHSS was implanted in the right incisions. Due to the different sample volume, the corresponding required incisions for EHSS-PT-130 group and EHSS group was 4 mm and 12 mm, respectively. The subcutaneous tissue was separated, and then the samples were implanted along the incision

gently into the subcutaneous tissue of rats, the rat skin incisions were seamed with surgical sutures finally. The rats were bred normally after the operation.

After the samples were implanted for 5, 15, 30 and 60 days, the rats back skin was cut and the EHSS-PT-130 and EHSS samples were taken out along with the surrounding tissues. The tissues were fixed, dehydrated with gradient ethanol (50%, 70%, 85%, 95%, and 100% (v/v) aqueous solution in sequence), embedded in paraffin for semi-thin sections, stained with hematoxylineosin (HE) and observed by optical microscope. Part of the samples were fixed with 2.5wt% glutaraldehyde for 12 h, and dehydrated with the above gradient ethanol and frozen in liquid nitrogen. Their surfaces were coated with gold, observed and photographed with SEM. All animal experimental procedures were carried out in accordance with the Guidelines and Regulations for Care and Use of Laboratory Animals based on the Experimental Animal Management Ordinance (National Science and Technology Committee of the People's Republic of China, 1998) and with the Guideline for Care and Use of Laboratory Animal of Wuhan University. The experiments were approved by the Animal Ethics Committee of School of Basic Medical Sciences of Wuhan University and carried out in Wuhan University Laboratory Animal Center.

2.7 Statistical analysis

All of the quantitative data were expressed as the mean ± standard deviation. Statistical comparisons were performed using one-way ANOVA with PASW 17.0 software (SPSS Incorporated, Chicago, IL). $P < 0.05$ was considered statistically significant.

3. Results and discussion

3.1 Effects of treatments on the micro-structure and shape memory property of EHSS

Effects of pressure, temperature, hot-pressing and its cycles on the recovery of EHSS were studied systematically. Fig. 1A shows the photographs of the original EHSS sponge, EHSS-PT-130, and recovered EHSS. The EHSS sponge showed a fluffy state before hot-pressing, which changed to a dense thin disk (EHSS-PT-130) by hot-pressing. After soaking in water, the thin disk could recover its original fluffy state as shown in “Recovered EHSS”. This is due to good hydrophilicity of HEC and SPI as well as relative stable cross-linking structure[29], which endowed EHSS water responsive shape memory ability[31].

So EHSS-PT-130 exhibited fascinating shape-memory function, which could be easily triggered by water. Moreover, the mechanical properties of the EHSS at dry (in air) and wet states were tested, and the results are shown in Fig. S1. EHSS at dry state exhibited relative high compressive strength of about 0.6 MPa, which decreased to about 0.4 MPa after water absorption. And the strain increased from 55.8% to 93.0% after water soaking. So water could decrease the compressive strength while increase the compressive strain at the same time. This means the water-soaked EHSS could be deformed more easily or pressed adaptable, which could endow EHSS-PT-130 with water responsive ability.

Compared with z dimension (thickness), the x and y dimension change for the sponges before and after treatment were relatively small (Figure 1A), so we only focused on the change of the thickness (z dimension) in this work. Figure 1B shows the thickness retention ratio and recovery ratio (percentage) of the EHSS sponges after different treatments. Obviously, the thickness retention ratio of EHSS decreased obviously from 7.8% to 4.1% with the increase of pressure from 5 MPa to 45 MPa (Fig. 1B, a) due to their fluffy sponge structure. After water soaking, the sponge thickness ratio could recover more than 98% for EHSS-P-n (n=5, 15, 30 and 45), showing good shape-memory property. The sponge thickness remained almost unchanged after hot treatment and water soaking (Fig. 1B, b) because EHSS exhibited certain structure stability through the ECH crosslinking and relative low coefficient of thermal expansion from biopolymers[31], showing good temperature stability. Under the constant pressure of 30 MPa, the thickness retention rate decreased slightly from 4.8 % to 4.0% with the increase of temperature from 30 to 210 ^{o}C (Fig. 1B, c). Interestingly, the recovery ratio changed from about 99% to 94% with the increase of hot-pressing temperature from 30 to 130 ^{o}C after soaking in water, so EHSS exhibited excellent shape-memory properties after hot-pressing with the temperature ≤ 130 ^{o}C and the pressure of 30 MPa. With the further increase of temperature to 170 ^{o}C, the recovery ratio of EHSS could reach about 80% because temperature at 170 ^{o}C could possibly affect the macromolecular structure to a small degree. Moreover, the recovery ratio decreased sharply to about 6% at 210 ^{o}C, so EHSS-PT-210 had low shape memory ability because high temperature could possibly decompose biopolymers, further break the original crosslinking

structure and even form new cross-linkingto some content. The recovery ratio was about 94% after the first cycle of the hot-pressing at 130 °C and 30 MPa pressure, which remained almost unchanged (above 99% of EHSS-C-1 after two cycles and EHSS-C-2 after three cycles, respectively) for EHSS-C-2 and EHSS-C-3 compared with EHSS-C-1, indicating good repeatability. Therefore, single pressure (≤ 45 MPa) or temperature (≤ 210 °C), hot-pressing condition of relative low temperature (≤ 130 °C) and its cycles had little effect on the recovery ratio of EHSS, and the hot-pressed EHSS (temperature ≤ 130 °C, pressure ≤ 30 MPa) exhibited good water responsive shape-recovery property, which could be used repeatedly for at least 3 times.

3.2 Effect of treatments on the structure of the EHSS sponge

Fig. 2 shows the FTIR spectra of EHSS after different hot-pressing treatments. The bands at around 3400 and 2926 cm^{-1} for all EHSS-P-n were assigned to the stretching vibrations of –OH and –CH for SPI and HEC, and the peaks at 1539 and 1234 cm^{-1} were attributed to the bending vibration of –NH for SPI (Fig. 2a). The peak positions were almost the same for EHSS at different pressure because crosslinked molecular structure exhibit stability against pressure. The peaks for the stretching vibrations of –OH shifted from 3399 cm^{-1} for EHSS-T-30 to 3406 and 3419 cm^{-1} for EHSS-T-130 and EHSS-T-210 respectively (Fig. 2b), because high temperature could remove the residual water in the sponges. The peak at 1312 cm^{-1} was assigned to the C-O stretching vibration, which almost disappeared in EHSS-T-210 because of the possible occurrence of certain carbonization at 210 °C (Fig. 2b). The changes were similar for EHSS-PT-30, EHSS-PT-130 and EHSS-PT-210 in Fig. 2c. There was no obvious change occurred from EHSS-C-1 to EHSS-C-3 (Fig. 2d), further confirming EHSS structure stability against the repeated hot-pressing treatment at 130 °C with the pressure of 30 MPa.

Fig. 2e shows the XRD patterns of EHSS after different treatments. Two main peaks at 2θ = 10.5 and 19.9° appeared in all the patterns, which were different from SPI and HEC[26], indicating the successful chemical crosslinking by ECH. EHSS-P-5 and EHSS-C-1 exhibited similar characteristic peaks with EHSS-P-45 and EHSS-C-3, respectively, indicating pressure and repeated hot-pressing treatment had little effect on their structure.

Compared with EHSS-T-30 and EHSS-PT-30, the peak intensity of EHSS-T-210 and EHSS-PT-210 decreased obviously respectively, indicating that the heating or hot-pressing treatments could possibly decrease the crystallinity by breaking the original crosslinking structure or inducing rearrangement of molecules[32,33]. Fig. 2f shows the TG curves of EHSS, SPI and HEC. There was nearly no weight loss for all curves in the range of 100-170 °C, confirming almost no decomposition occurred and their structure stability below 170 °C. Weight loss values of 1.1%, 0.8% and 2.0% were measured during the range of 170-210 °C for EHSS, SPI and HEC respectively, indicating certain molecular decomposition. Thus, 170 °C temperature had little effect on the structure of EHSS, but 210 °C temperature could affect the EHSS structure due to possible occurrence of certain carbonization, which was consistent with the FTIR and XRD results.

3.3 The morphology change of the EHSS sponge on the micro scale

Fig. 3 shows the SEM images of the surface and cross-section morphologies of EHSS, Treated EHSS after pressing at different pressures (Temperature, 30 °C) and the corresponding Recovered EHSS. The corresponding average pore sizes or the number of micro-gaps among flattened pore walls (Figure 3a) were calculated by a piece of software "nanomeasurer 1.2". EHSS surface exhibited homogenous porous structure with the pore size of about 200 μm (Fig S2a), which is very important for cell adhesion and nutrient exchange[20]. Obviously, the above pores subsided to form relative dense structure with some micro-gaps among pore walls after pressing on the surface, and the pore shape changed from "regular" to "flattened", and the average pore size decrease from 104.2 μm to 68.9 μm with the increase of the pressure (Fig. 3a, EHSS, Treated EHSS). The porous structure and pore shape recovered with the average pore size of 150.0 μm (Fig S2a) after water soaking for all EHSS-P-n sponges (n=5, 15, 30 and 45) (Fig. 3a, Recovered EHSS) because water could permeate through the micro-gaps on the surface and cross-section to swelling HEC and SPI molecules (Fig. 3a, EHSS, Treated EHSS), showing good shape-memory property on the micro scale. There were also similar homogenous pores with the average pore size of about 150 μm (Fig S2b) appeared on the cross-section of EHSS (Fig. 3b, EHSS), indicating an interconnected porous structure. The porous structure on the cross-section changed to

relative dense structure after pressing and was similar with that on the surface (Fig. 3b). Moreover, the thickness of EHSS sponges decreased clearly with the increase of the pressure (Fig. 3b, Treated EHSS), indicating that the compactedness of Treated EHSS increased with the pressure. Obviously, Treated EHSS with higher compactedness was harder for water permeation. The porous structure of the cross-section could also recover well with the average pore size of about 136 μm (Fig S2b) after water soaking, showing excellent shape-memory property on the micro scale (Fig. 3b, Recovered EHSS).

Fig. 4 shows the SEM images of the surface and cross-section morphologies of the EHSS sponges, Treated EHSS after hot-pressing at different temperatures (Pressure, 30 MPa) and the corresponding Recovered EHSS. Obviously, the surface "regular" pores with the average pore size of about 180 μm (Fig S2c) were flattened after hot-pressing (Fig. 4a, EHSS, Treated EHSS). The surface roughness of Treated EHSS and the number of the micro-gaps decreased with the increase of temperature. The surface of EHSS-PT-210 became very smooth and all the pores wall merged tightly to form an entire part with nearly no micro-gaps because the soy protein molecules exhibit removability at high temperature, namely thermoplasticity[34], so the soy protein molecules could move gradually to form dense structure at high temperature and pressure. The porous structure recovered well at the temperature ≤130 ^{o}C possibly due to the water permeable structure on the surface and cross-section, most of the pores recovered at 170 ^{o}C (Fig. 4a, Recovered EHSS), which was in accordance with Fig. 1B, c. Moreover, surface pores couldn't recover at 210 ^{o}C, only small gaps appeared on the surface due to water impermeable structure on the surface and cross-section, confirming the results shown in Fig. 1B-c on the micro scale. With the increase of hot-pressing temperature, the cross-section of the EHSS sponges become denser, and the thickness decreased accordingly due to the thermoplasticity of soy protein. Thus, EHSS thickness could be controlled by hot-pressing treatment. After water soaking, the porous structure with the average pore size of about 123 μm (Fig S2d) recovered well for the EHSS-PT-n (n=30, 90, 130, and 170) (Fig. 4b, Recovered EHSS). Undoubtly, the porous structure couldn't recover for the hot-pressing temperature at 210 ^{o}C because high temperature could break the original structure through the decomposition of biopolymers

and the change of crosslinking structures severely with the pressure of 30 MPa to form water impermeable structure (Fig. 4b, EHSS-PT-210), which surpassed water responsive shape memory ability of EHSS.

3.4 Effects of hot-pressing process on the relative water absorption ratio and sterilization efficiency of EHSS

Water absorption ability was closely associated with the sponge structure, so the water absorption ability could reflect the structure change. Fig. 5 shows the result of the relative water uptake ratio values (RWU) after pressing and hot-pressing treatments. The water uptake ratio of EHSS (EHSS-P-0) before treatment was used as the control (100%). Interestingly, the RWU of EHSS-P-5 was slightly higher than 100%, so 5 MPa pressure had nearly no effect on its structure. Obviously, the RWU decreased with further increase of pressure (15, 30 and 45 MPa), and the RWU for EHSS-P-15, EHSS-P-30 and EHSS-P-45 were about 80% (Fig. 5a), showing good resistance to the applied pressure. The RWU also decreased with the increase of the applied temperature because the number of the micro-gaps on Treated EHSS decreased with temperature, which had adverse effect on water absorption (Fig. 4a, Treated EHSS). The RWU could still remain above 66% in the range of 30-170 ^{o}C, which were smaller than that of EHSS-P-n due to the thermoplasticity of soy protein. The RWU was just about 5% for EHSS-PT-210, because the porous structure was broken severely at 210 ^{o}C (Fig. 4, EHSS-PT-210). Therefore, Treated EHSS could retain most of original water absorption ability at temperature ≤170 ^{o}C. Moreover, the RWU of EHSS and EHSS-PT-130 at different time intervals were also studied to evaluate the effect of hot-pressing on the swelling kinetics (Fig S3). The RWU of EHSS-PT-130 could reach 64% and 69% at 0.5 and 1 d, respectively, indicating relative quick water absorbability to ensure its good water responsive shape-recovery property.

Fig. S4 shows the sterilization effect of different hot-pressing treatments on EHSS. There was yellow bacterial colonies appeared on the bottom of the EHSS-PT-30, and “irregular” bacterial colonies appeared around EHSS-PT-90 (Fig. S4, EHSS-PT-30 and EHSS-PT-90), indicating that bacteria in the sponges were not totally sterilized and still remained alive in the sponges. Inspiringly, there was no bacterial colony appeared on the culture palates for

EHSS-PT-130, EHSS-PT-170 and EHSS-PT-210, and no new bacterial colony appeared after the following culture of 72 h, indicating that bacteria was totally sterilized during the hot-pressing process at the temperature $\geqslant$ 130 °C (Fig. S2). Thus, the hot pressing process ($\geq$ 130 °C) could be used for complete sterilization directly without additional autoclaved sterilization, which is suitable for commoditized storage and transportation, and the resultant hot-pressed EHSS could be used directly after opening the packages.

3.5 Cytocompatibility evaluation of the hot-pressed EHSS sponges

Fig S5a shows the cell viability of L929 cells in the extracts from EHSS and all the hot-pressed sponges. The cell viability values of EHSS and EHSS-30 or EHSS-90 and EHSS-130 were slightly higher than or close to that of the control because SPI hydrolysate in extracts could promote cell growth and proliferation, respectively. With the further increase of the hot-pressing temperature, the cell viability of EHSS-PT-170 decreased to about 72% possibly due to certain molecular decomposition, showing low cytotoxicity. It was noted that the cell viability of EHSS-PT-210 decreased to 59% possibly due to the occurrence of certain carbonization (Fig. 2f), showing relative high acute cytotoxicity. Therefore, the overall viability of the cells for the hot-pressing temperature $\leqslant$ 170 °C was in the normal range, showing no or low cytotoxicity. In this work, L929 cells were transfected with green fluorescent protein (GFP) for direct observation under fluorescence[35]. Fig. 6 shows the photographs of the transfected L929 cells cultured with EHSS-PT-n. Obviously, L929 cells could adhere and grow normally all over EHSS-PT-n (n = 30, 90 and 130) including the surface and interior, further confirming their recoverable interconnected macro-porous structure. The L929 cells on EHSS-PT-n (n = 30, 90 and 130) exhibited shuttle-shape, indicating their nontoxicity and good cytocompatibility[36]. The confocal image of the pure EHSS-PT-210 sponge without cells has been added in the Supplementary Material (Fig S5b). Obviously, EHSS-PT-210 itself could fluoresce possibly due to certain carbonation effect at 210 ºC high temperature[37]. Even many “green” substances have been observed (Fig. 6, EHSS-PT-210), but there were few “green” substances with cell morphologies were observed (especially shuttle-shape) on EHSS-PT-210, possibly because the relative smooth and dense surface of EHSS-PT-210 was not good for cell adhesion and

cell proliferation. This was proven by the MTT assay results as shown in Fig. S5a, the extract of EHSS-PT-210 had relative high acute cytotoxicity.

Fig. 7 shows the corresponding SEM images of L929 cells directly cultured with the EHSS-PT-n. As it was expected, the EHSS-PT-n (n= 30, 90 and 130) could recover their original interconnected porous structure during cell culture process, further confirming their good shape-memory property (Fig. 7, EHSS-PT-30-170). However, the EHSS-PT-210 sponge couldn't recover its original porous structure (Fig. 7, EHSS-PT-210), which was consistent with the result from Fig. 4a. Similar to the results of fluorescent photographs (Fig. 6, EHSS-PT-30-130), L929 cells could adhere and grow well on the surface and in the interior of Treated sponges, most of which exhibited shuttle-shape like those in the control. There was almost no cells adhered on EHSS-PT-210, which was also consisted with the result of the confocal photographs due to its fluid impermeable structure (Fig. 4a and Fig. 7, EHSS-PT-210).

3.6 Subcutaneous defect filling and repair evaluation

Shape memory EHSS-PT-130 had relative low thickness retention ratio and good recovery ratio (Fig. 1B, c), so the filling and repair of the same soft tissues defect required the smallest surgical incision for EHSS-PT-130. Moreover, EHSS-PT-130 exhibited good cytocompatibility without the need of extra sterilization (Fig. S4, 6 and 7), so EHSS-PT-130 was selected for subcutaneous defect filling and repair to compare with original EHSS. Fig. 8a shows the photographs of simultaneous subcutaneous filling surgery of EHSS-PT-130 and EHSS. The thin disk of EHSS-PT-130 could be facilely curled up into a cylinder, and EHSS was a thick block, obviously, the surgical incision for EHSS-PT-130 (4 mm) was much smaller than that for EHSS sponge (13 mm) (Fig. 8a), so the damage to the skin and the corresponding scar would be much smaller. Interestingly, EHSS-PT-130 recovered its original porous structure very quickly from the observation, which would achieve almost the same effect with EHSS. Computed Tomography (CT) could be used to measure the area of inner defected soft tissue, so we could calculate the size of EHSS that could be used for the corresponding repair. EHSS with required sizes which could then be hot-pressed to reduce the thickness for the effective reduction of the corresponding surgical incision compared

with original EHSS. Thus, the application of EHSS-PT-130 greatly reduced the surgical incision without sacrificing any repair effect.

The in vitro degradation ratio of EHSS in PBS was evaluated and shown in Fig. S6. EHSS could be degraded gradually with longer incubation time. EHSS could be degraded at 3d, and its degradation ratios reached 11.4% and 19.0% at 7 d and 14 d, respectively. With longer incubation time, the degradation ratio of EHSS reached 39.3%, showing relative good in vitro degradability. In order to further study the effect of the hot-pressing process on the *in vivo* recovery ratio and histocompatibility, EHSS-PT-130 and EHSS were implanted *in vivo*. Fig. 8b shows the thickness percentage (recovery ratio) of EHSS and EHSS-PT-130. The thickness ratio (percentage) of EHSS after 5 days implantation was 83.8% of original EHSS due to the natural pressure from rat skin. And the thickness ratio (percentage) for EHSS-PT-130 was 81.5% after 5 days implantation, which was close to that of EHSS sponge, indicating the similar filling function with EHSS. Owing to the biodegradation, the thickness ratios of EHSS-PT-130 decreased to 78.0 % and 70.7 % after implantation for 15 and 30 days, respectively. Obviously, these thickness ratios were also similar to those of EHSS sponge (80.3% and 68.0%), further confirming the similar effect with EHSS. Fig. 9a shows the HE photographs of EHSS-PT-130 and EHSS after implanted in the rats. After 5 days, cells could infiltrate and grow in the interior of EHSS-PT-130 and EHSS, the sponge skeleton remained intact with some scatteredly distributed inflammatory cells. Abundant cells grew and aggregated in the interior of the EHSS-PT-130 and EHSS sponges after 15 days with their degradation[38]. The sponges were surrounded by the tissue with a large number of cells proliferated in the interior of the materials after implanted for 30 days, most of sponge material skeleton broke with less inflammatory cells remained around, showing better compatibility with cells and tissue. The sponge materials combined tightly with the cells and tissue after 60 days and the regenerated tissue occupied the sites of the original sponges gradually, and there was no obvious boundaries and differences between sponges and the surrounding mucosa and mucosal muscular tissue[39].

Fig. 9b and Fig. S7 show the corresponding SEM images of EHSS-PT-130 and EHSS . EHSS-PT-130 could recover the inter-connected porous structure after 5 days, which was

similar to that of EHSS. Cells started to infiltrate inside the sponges, and there was almost no cells appeared in some parts of the interior of sponges, indicating that cell infiltration process was from outside to inside (Fig. 9b). The sponges and the tissue combined gradually with the extension of time, cells infiltrated in the interior of the sponges and grew accumulatively to form tissue and occupy the original sites of the sponges accompanied with their degradation gradually (Fig. S7). Cells infiltrated in the interior of the sponges totally and began to aggregate after 15 days, which grew accumulatively and the newly formed tissue aligned with sponges completely after 30 days. More and more regenerative tissue formed and went into the sponge with the degradation of the sponge, AND the spongescould be completely biodegraded in vivo at 60 days and As a result, only the regenerative tissue could be observed in SEM images after 60 days, which occupied the space of original sponges on the whole. Therefore, the EHSS and EHSS-PT-130 showed almost no difference and both exhibited good histocompatibility and were completely biodegradable *in vivo*.

4. Conclusions

Novel EHSS with shape memory characteristics were constructed successfully through a blending, crosslinking and freeze-drying process, whose thickness could be controlled by hot-pressing treatments. EHSS could be pressed into thin disks with much smaller thickness. Especially the resultant disk (EHSS-PT-130) obtained in suitable condition at 130 ^{o}C with the pressure of 30 MPa could quickly recover its original shape by soaking in hydrophilic fluids on the macro and micro scales, showing water responsive shape memory property. EHSS could be totally sterilized by hot-pressing process with the temperature ≥ 130 ^{o}C. The thickness retention ratio and recovery ratio were affected by hot-pressing conditions such as pressure and temperature. EHSS-PT-130 exhibited good cytocompatibility, histocompatibility and *in vivo* biodegradability, which was almost the same with EHSS. Compared with original EHSS, shape memory and hydrophilic EHSS-PT-130 required much smaller surgical incision and no need of extra sterilization to reach the same repair effect, showing potential application as the filling and repair biomaterials for soft tissue defect.

Acknowledgements.

This work was supported by the National Natural Science Foundation of China (Grant Nos: NSFC 81471789, NSFC 81171480 and NSFC 51503177) and Fundamental Research Funds for the Central Universities (Grant No. 2042014kf0253 and 2042014kf0271).

References

1 H. Yu, X. Chen, J. Cai, D. Ye, Y. Wu, L. Fan, P. Liu, Chem. Eng. J. 2019, **369**, 253–262.

2 P. N. Wells, H. D. Liang, *J. Royal. Soc. Interface,* 2011, **8**, 1521-1549.

3 R. C. Rui, A. M. S. Costa, S. G. Caridade, J. F. Mano, Chem. Mater. 2015, 27, 7490-7502.

4 A. Limaye, Soft Tissue Repair Market by Product (Mesh/Tissue patch, Allograft, Xenograft, Suture Anchor, Interference Screws, Laparoscopic Instruments) by Application (Hernia, Dural, Orthopedic, Skin, Dental, Vaginal, Breast augmentation)-Global Forecast to 2019, *Markets and Markets*: 2015.

5 A. Nair, Y. T. Tsai, K. Shah, J. Shen, H. Weng, J. Zhou, X. Sun, R. Saxena, J. Borrelli, L. Tang, *Biomaterials*, 2013, **34**, 7364-7371.

6 N. Soffertsur, M. Shevach, A. Shapira, D. Peer, T. Dvir, *Biofabrication,* 2014, **6**, 035023-035023.

7 A. Colletta, J. Wu, Y. Wo, M. Kappler, H. Chen, C. Xi, M. E. Meyerhoff, *ACS Biomater. Sci. Eng.,* 2015, **1**, 416−424.

8 P. Li, S. Jiang, Y. Yu, J. Yang, Z. Yang, *J. Mech. Behav. Biomed.,* 2015, **49**, 220-234.

9 E. J. Olson, C. D. Harner, F. H. Fu, M. B. Silbey, *Orthopedics,*1992, **15**, 1225-1232.

10 A. Giedraitis, S. P. Arnoczky, A. Bedi, *Sport Health*, 2014, **6**, 256-264.

11 M. Fan, Y. Ma, J. Mao, Z. Zhang, H. Tan, *Acta Biomater.,* 2015, **20**, 60-68.

12 L. Z. Linan, N. M. Nascimento Lima, R. M. Filho, M. A. Sabino, M. T. Kozlowski, F. Manenti, *Mat. Sci. Eng. C,* 2015, **51**,107-116.

13 J. C. Min, D. W. Kim, J. K. Yun, H. Y. Kweon, Y. J. Cho, S. Y. Choi, H. R. Lee, *Mol. Cell. Toxicol,.* 2014, **10**, 277-283.

14 Y. Ramadan, M. I. Gonzálezsánchez, K. Hawkins, J. Rubioretama, E. Valero, S. Perni, P. Prokopovich, E. Lópezcabarcos, *Mat. Sci. Eng. C,* 2014, 42, 696-704.

15 J. Xu, W. Zhu, L. Jiang, J. Xu, Y. Zhang, Y. Cui, *RSC Adv.,* 2015, 5, 72736-72744.

16 V. Agrawal, P. S. Almond, R. Reyna, M. A. Emran, Case Rep., 2015, **49**, 230-233.

17 F. Rupp, D. Axmann, C. Ziegler, J. Geis-Gerstorfer, *J.Biomed. Mater. Res. A*, 2002, **62**, 567-78.

18 B. A. Aderibigbe, Design and Application of Injectable Gels in Tissue Engineering and Drug Delivery, Springer: 2018; p 311-339.

19 J. Rnjakkovacina, L. S. Wray, K. A. Burke, T. Torregrosa, J. M. Golinski, W. Huang, D. L. Kaplan, *ACS Biomater. Sci. Eng.,* 2015, 1, 260-270.

20 A. M. Hawkins, T. A. Milbrandt, D. A. Puleo, J. Z. Hilt, *J.Biomed. Mater. Res. A*, 2014, **102**, 400-412.

21 Z. Yang, H. Jiang, S. H. Ye, T. Yoshizumi, W. R. Wagner, *Biomaterials*, 2015, **53**, 484-493.

22 S. Wu, X. Liu, K. W. K. Yeung, C. Liu, X. Yang, *Mat. Sci. Eng. R,* 2014, 80, 1–36.

23 Y. Zhao, M. He, H. Jin, L. Zhao, Q. Du, H. Deng, W. Tian, Y. Li, X. Lv, Y. Chen, *Chem. Eng. J.,* 2018, **341**, 402-413.

24 T. Muthukumar, D. Prakash, K. Anbarasu, B. S. Kumar, T. P. Sastry, *RSC Adv.,* 2014, **4**, 64267-64276.

25 Y. Pei, D.Ye, Q. Zhao, X. Wang, C. Zhang, W. Huang, N. Zhang, S. Liu, L. Zhang, *J. Mater. Chem. B,* 2015, **3**, 7518-7528.

26 Y. Guo, Z. Lv, Y. Huo, L. Sun, S. Chen, Z. Liu, C. He, X. Bi, X. Fan, Z. You, *J. Mater. Chem. B,* 2019, 7, 123-132.

27 Y. Xie, D. Lei, S. Wang, Z. Liu L. Sun, J. Zhang, F. Qing, C. He, Z. You, *ACS Biomater. Sci. Eng.,* 2019, **5**, 1668–1676.

28 J. G. Torres-Rendon, T. Femmer, L. L. De, T. Tigges, K. Rahimi, F. Gremse, S. Zafarnia, W. Lederle, S. Ifuku, M. Wessling, *Adv. Mater.,* 2015, **27**, 2989-2995.

29 Y. Zhao, M. He, L. Zhao, S. Wang, Y. Li, G. Li, M. Li, L. Xu, P. R. Chang, D. P. Anderson, Y. Chen, *ACS Appl. Mater. Interfaces,* 2016, **8**, 2781-2795.

30 J. S. Gonzalez, A. S. Maiolo, C. E. Hoppe, V. A. Alvarez, *Procedia Mater. Sci.,* 2012, **1**, 483-490.

31 A. V. Salvekar, W. M. Huang, R. Xiao, Y. S. Wong, S. S. Venkatraman, K. H. Tay, Z. X. Shen, *Accounts Chem. Res.* 2017, **50**, 141-150.

32 Q. Wang, J. Cai, L. Zhang, M. Xu, H. Cheng, C. C. Han, S. Kuga, J. Xiao, R. Xiao, *J. Mater. Chem. A,* 2013, **1**, 6678-6686.

33 K. Kamida, K. Okajima, T. Matsui, K. Kowsaka, *Polymer J.,* 1984, 16, 857-866.

34 Y. Yang, N. Reddy, Ind. Crop. Prod., 2012, **36**, 116–121

35 A. Svendsen, H. V. Kiefer, H. B. Pedersen, A. V. Bochenkova, L. H. Andersen, J. Am. Chem. Soc., 2017, **139**, 8766-8771.

36 M. He, Y. Zhao, J. Duan, Z. Wang, Y. Chen, L. Zhang, *ACS Appl. Mater. Interfaces,* 2014, **6**, 1872-8.

37 P. Shen, J. Gao, J. Cong, Z. Liu, C. Li, J. Yao, *ChemistrySelect*, 2016, **1**, 1314-1317.

38 L. H. Luo, Y. F. Zhang, X. M. Wang, Y. Wan, P. R. Chang, D. P. Anderson, Y. Chen, *J. Biomater. Appl.,* 2010, *24*, 503-526.

39 K. Burugapalli, J. C. Chan, J. L. Kelly, A. S. Pandit, *Macromol. Biosci.,* 2014, **14**, 244-256.

Figure Captions

Scheme 1 Treatment process of the sponges by pressing at 30 ºC, hot pressing or heating without pressure, and the corresponding sample codes.

Fig. 1. Photographs of EHSS, EHSS-PT-130 and the corresponding recovered EHSS by water soaking and freeze-drying process. The effects of different treatments on the change of thickness percentage ratios of treated EHSS (a: EHSS-P-n, n = 0, 5, 15, 30 and 45. b: EHSS-T-n, n = 30, 90, 130, 170 and 210. c: EHSS-PT-n, n = 30, 90, 130, 170 and 210. d: EHSS-C-n, n = 1, 2 and 3) and the corresponding recovered EHSS by water soaking and freeze-drying process to EHSS.

Fig. S1. The stress-strain curves of EHSS at dry and wet states (a) and the average compressive strength (b).

Fig. 2. FTIR spectra of EHSS-P-n (n = 5, 15, 30 and 45) sponges (a), EHSS-T-n (n = 30, 130 and 210) sponges (b), EHSS-PT-n (n = 30, 130 and 210) sponges (c) and EHSS-C-n (n = 1 and 3) sponges (d) , XRD patterns of EHSS-P-n (n = 5 and 45) sponges, EHSS-T-n (n = 30 and 210) sponges, EHSS-PT-n (n = 30 and 210) sponges and EHSS-C-n (n = 1 and 3) sponges (e), and TG curves of EHSS, SPI and HEC.

Fig. 3. SEM images of the surfaces (a) and cross-sections (b) of EHSS, Treated EHSS (pressed at 30 ºC with different pressure of n=5, 15, 30 and 45 MPa, EHSS-P-n) and the corresponding Recovered EHSS. Scale bar = 200 μm.

Fig. S2. The statistical size histograms of the average pore size for the surfaces of EHSS, Treated EHSS and the corresponding Recovered EHSS (a, c), and the corresponding cross-sections of EHSS and Recovered EHSS (b, d).

Fig. 4. SEM images of the surfaces (a) and the cross-sections (b) of EHSS, Treated EHSS (pressed at 30 MPa pressure with different temperature of n=30, 90, 130, 170 and 210 ºC, EHSS-PT-n) and the corresponding Recovered EHSS. Scale bar = 200 μm.

Fig. 5. Relative water uptake ratio of EHSS-P-n (n = 0, 5, 15, 30 and 45) sponges (a) and EHSS-PT-n (n = 30, 90, 130, 170 and 210) sponges (b).

Fig. S3. The swelling kinetics of EHSS and EHSS-PT-130 in ultrapure water.

Fig. S4. The photographs of bacteria survival status for the EHSS-PT-n (n = 30, 90, 130,

170 and 210) sponges.

Fig. 6. Confocal microscope images of GFP-transfected L929 cells cultured on the control and EHSS-PT-n (n = 30, 90, 130 and 210) sponges for 72 h. Scale bar = 50 μm.

Fig. S5. Cell viability of L929 cultured in extracts from the EHSS and EHSS-PT-n (n =30, 90, 170 and 210) sponges for 24h,48h and 72h. *P＜0.05, **P＜0.01 (compared with the control at the same time) (a), and confocal microscope image of pure EHSS-PT-210 without cells (b).

Fig. 7. SEM images of L929 cells cultured on the control and EHSS-PT-n (n = 30, 90, 130, 170 and 210) sponges for 72 h.

Fig. 8. Filling and repair process of rat tissues with EHSS-PT-130 (left) and EHSS sponges (right) (a), and thickness ratio of EHSS-PT-130 and EHSS sponges after implantation in rats for 5, 15 and 30 days (b).

Fig. S6. Dependence of *in vitro* degradation ratio of EHSS soaked in PBS on soaking time.

Fig. 9. HE photographs of the EHSS-PT-130 and EHSS sponges after implanted in rats for 5, 15, 30 and 60 days, respectively (a), and SEM images of EHSS-PT-130 and EHSS sponges after implanted in rats for 5, 15, 30 and 60 days (b), respectively.

Fig. S7. SEM images of EHSS-PT-130 and EHSS sponges after implanted in rats for 5, 15, 30 and 60 days (b) . Scale bar = 50 μm.

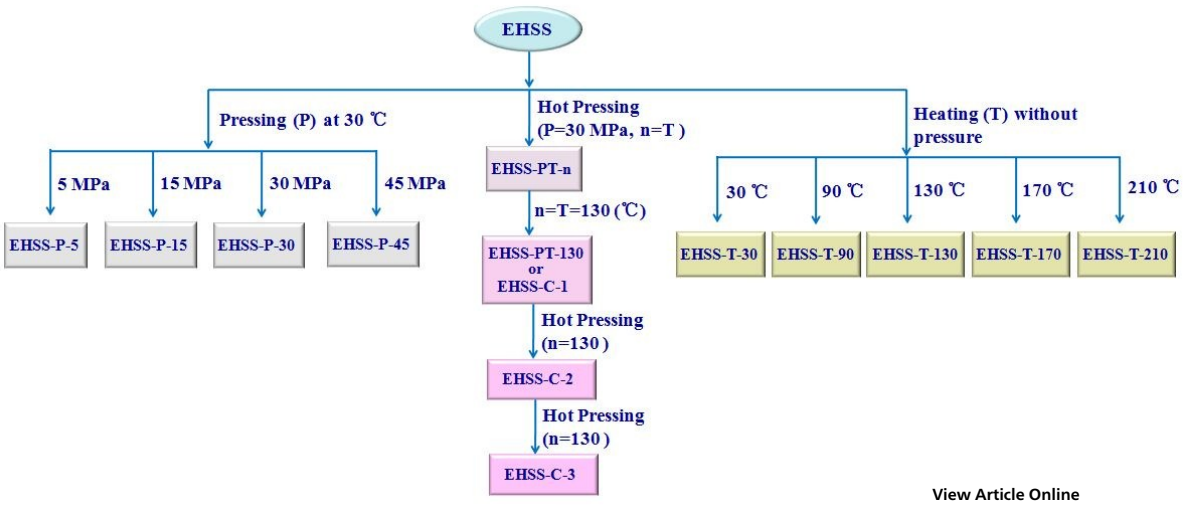

Scheme 1

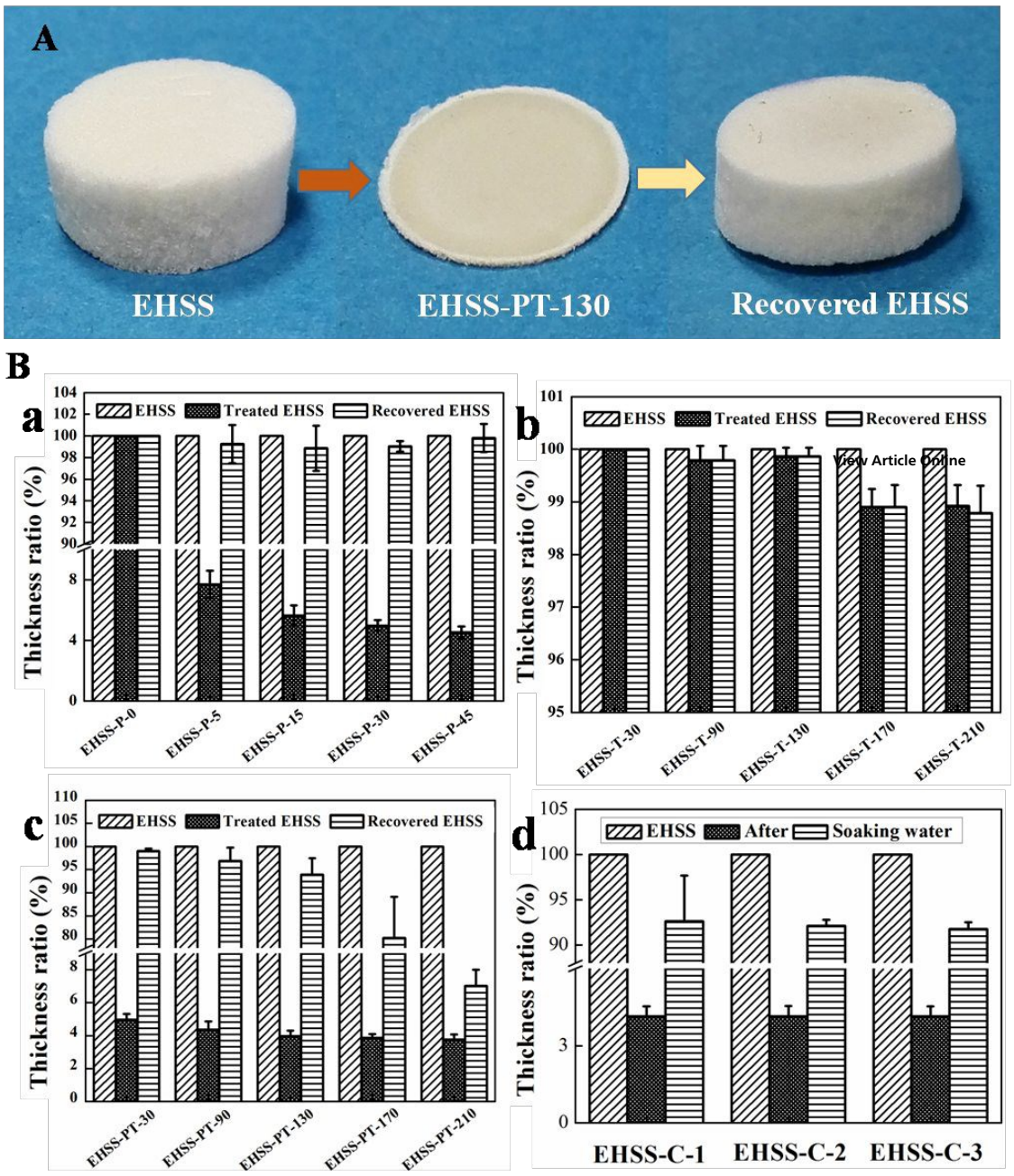

Fig. 1.

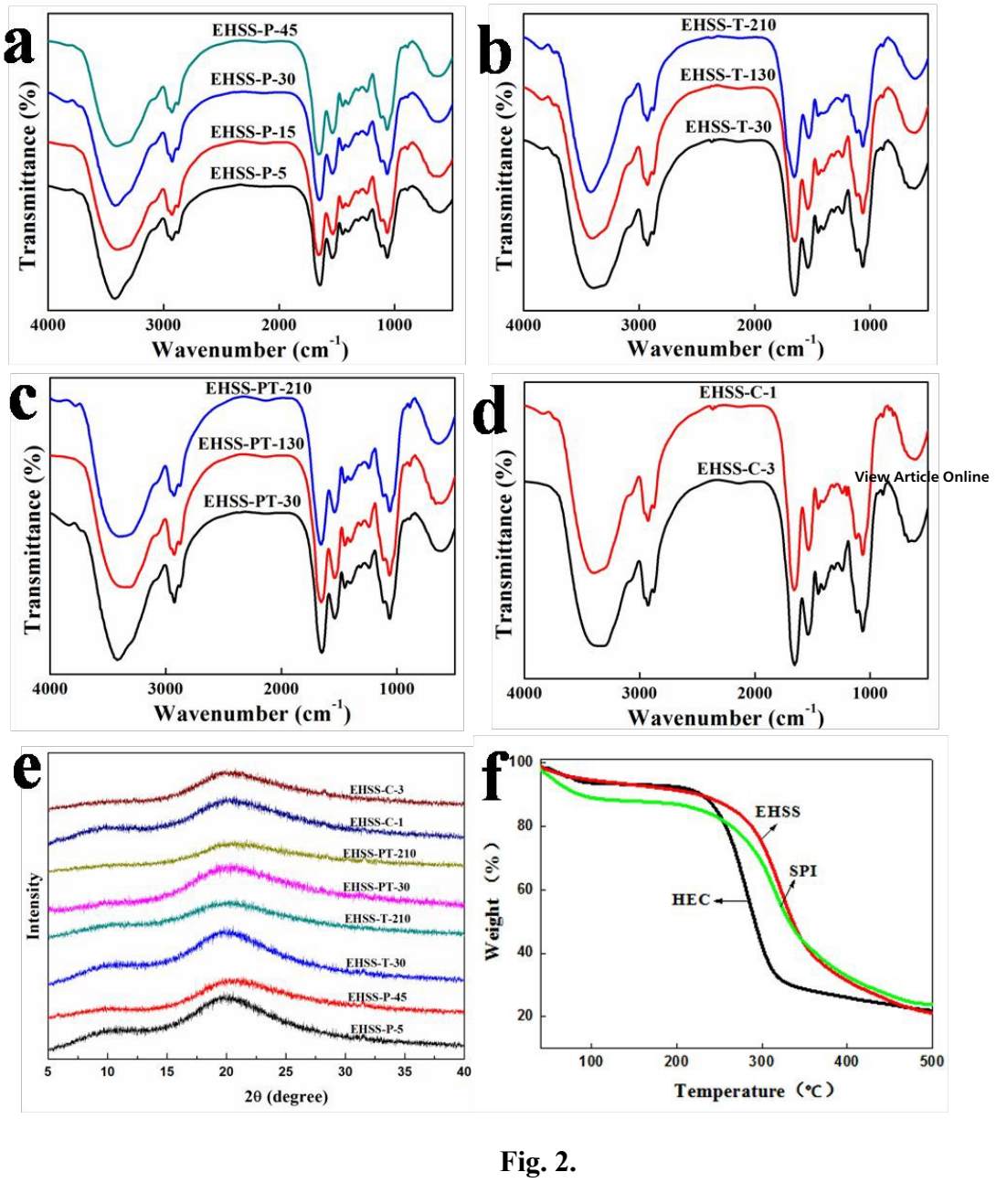

Fig. 2.

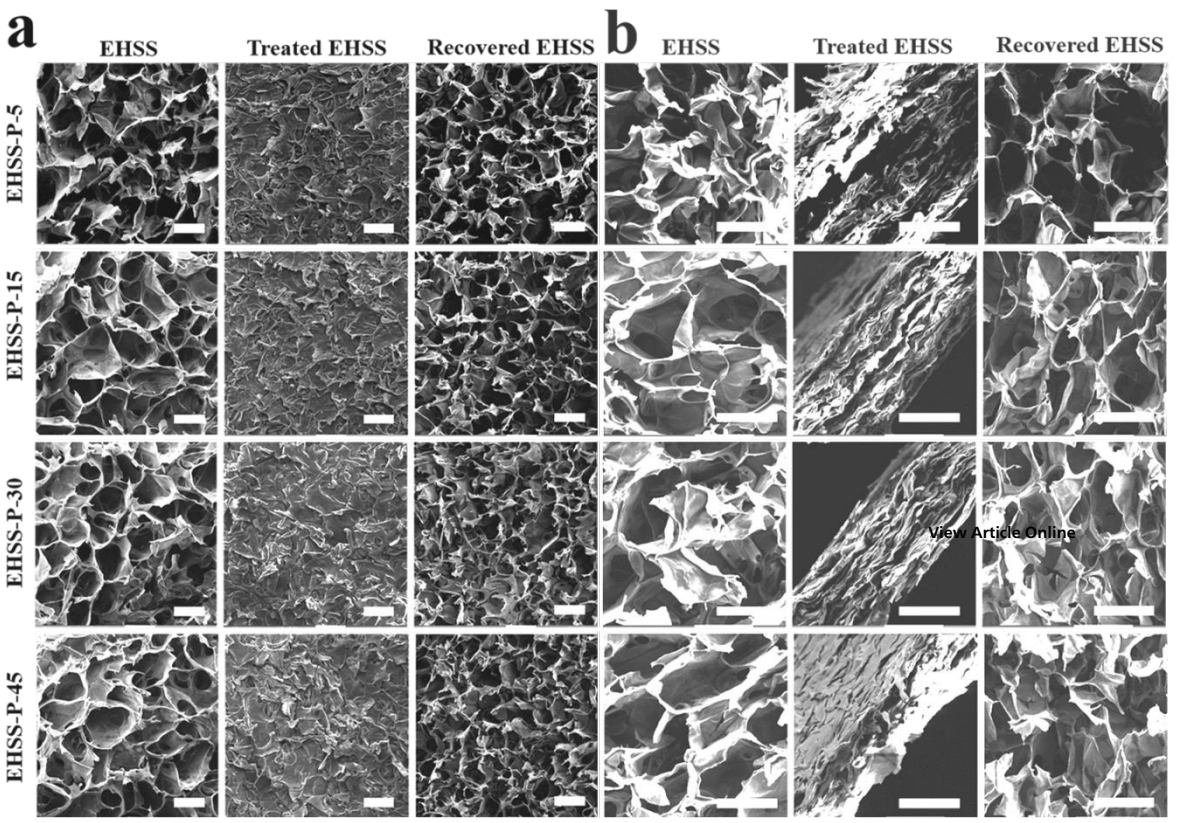

Fig. 3.

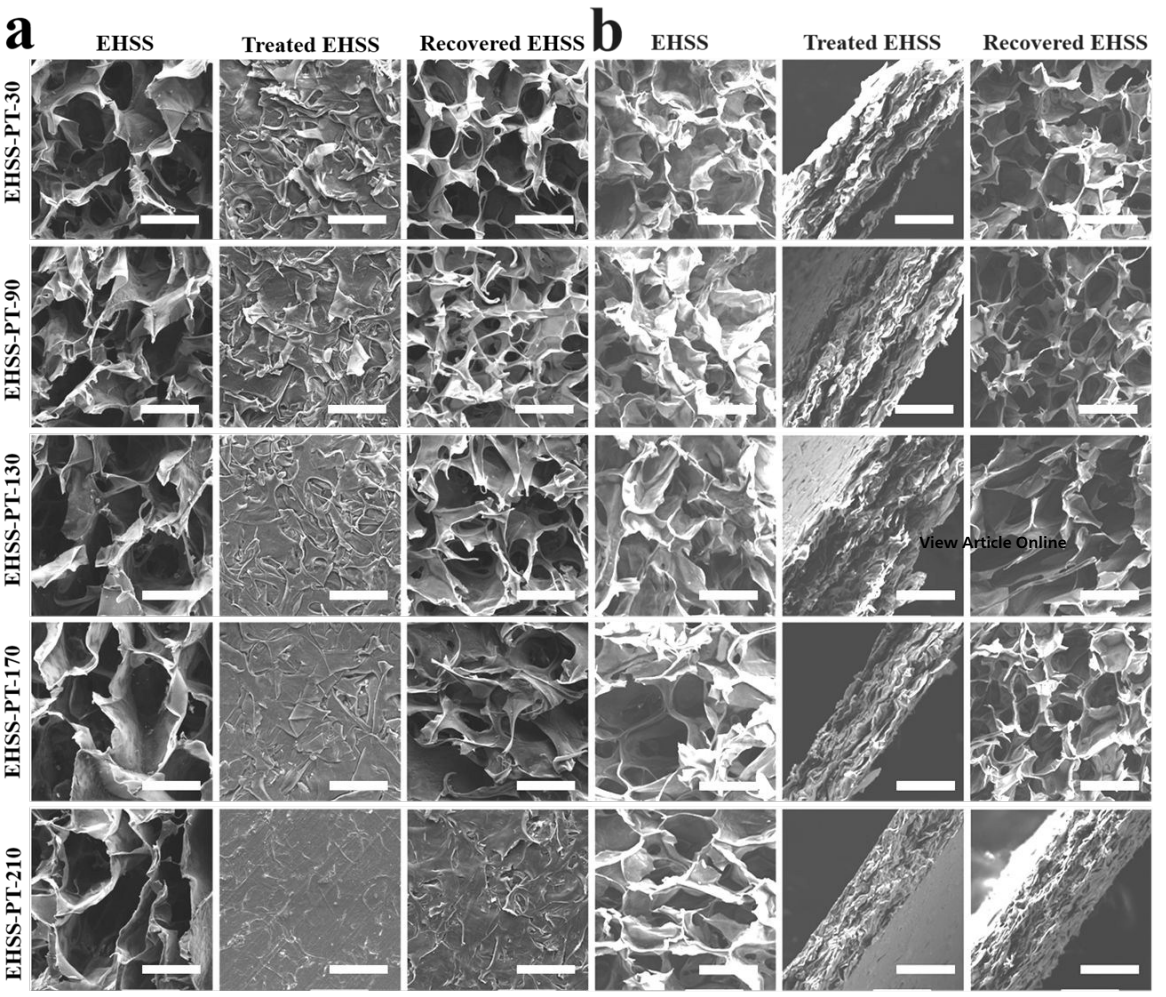

Fig. 4.

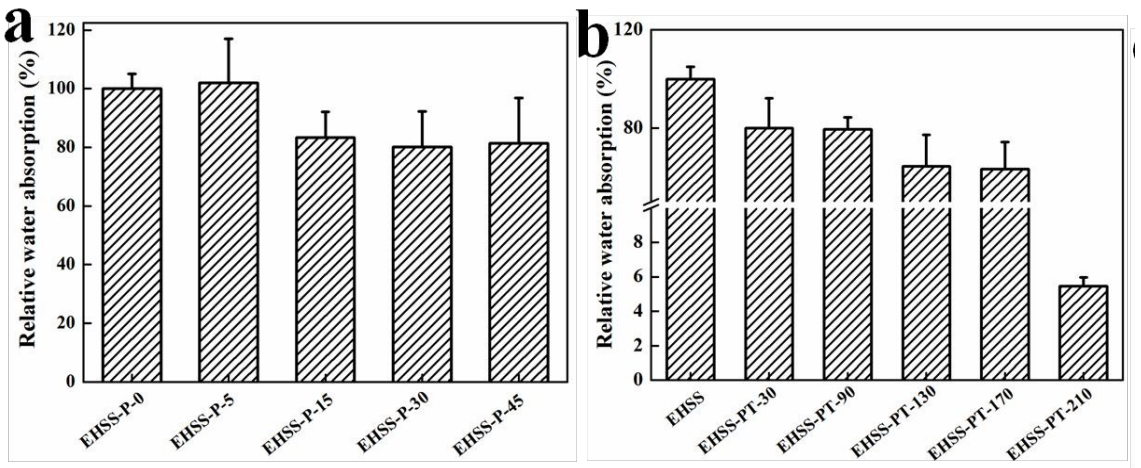

Fig. 5.

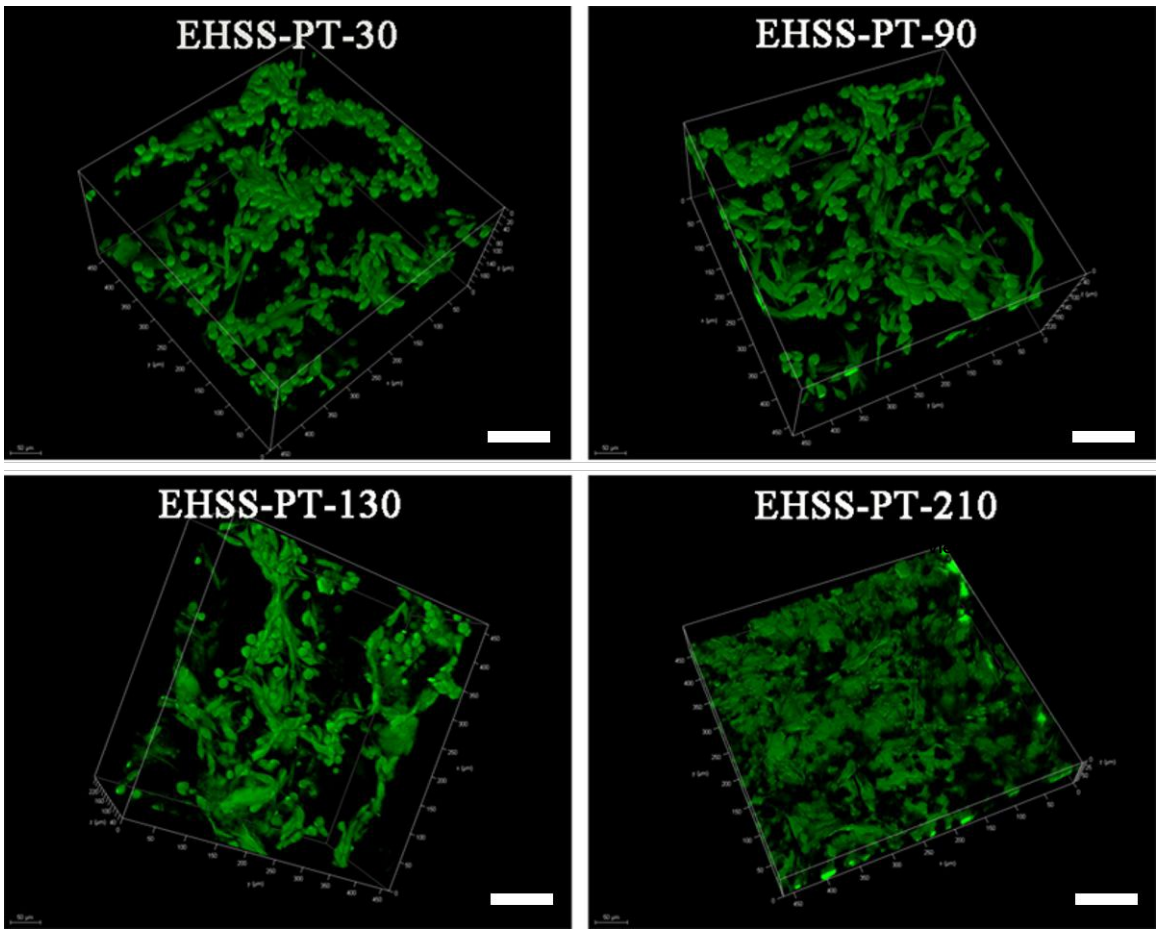

Fig. 6.

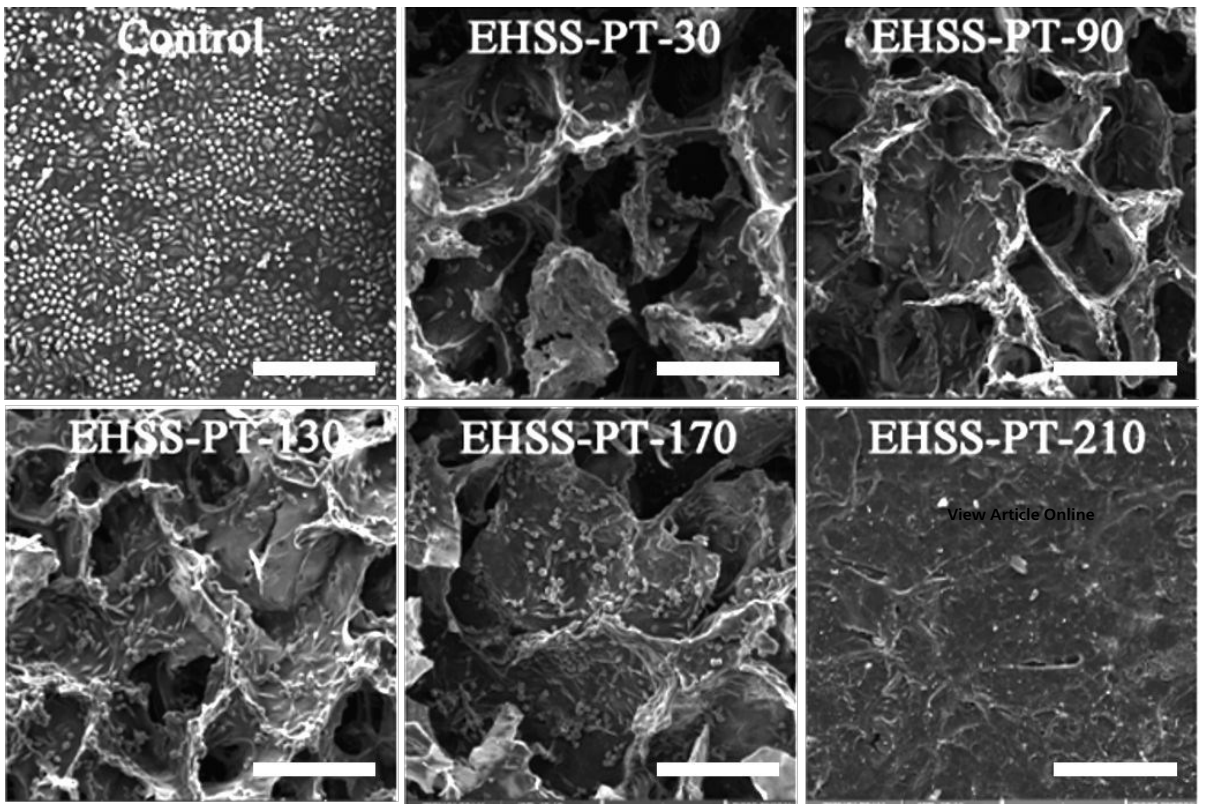

Fig. 7.

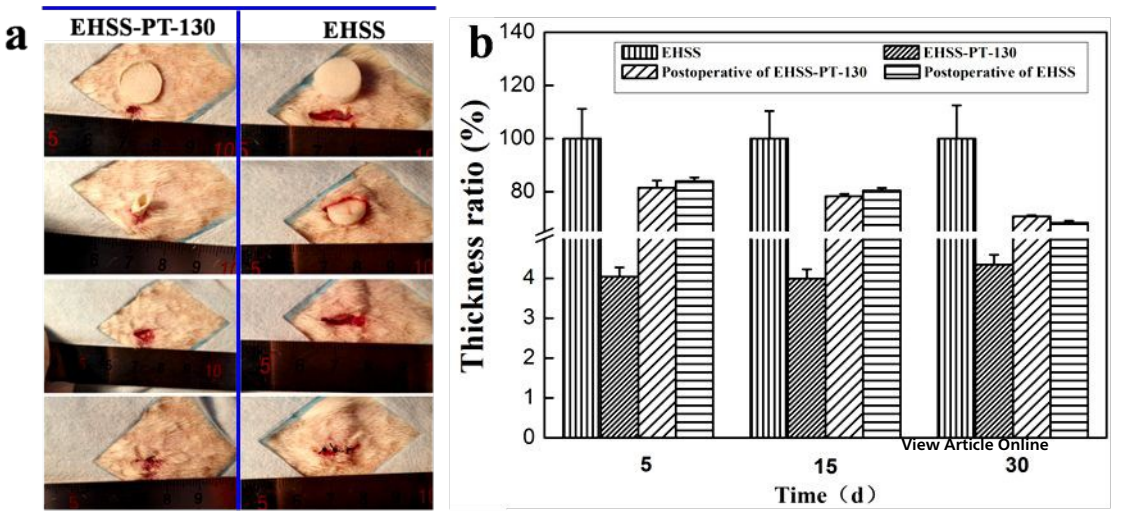

Fig. 8.

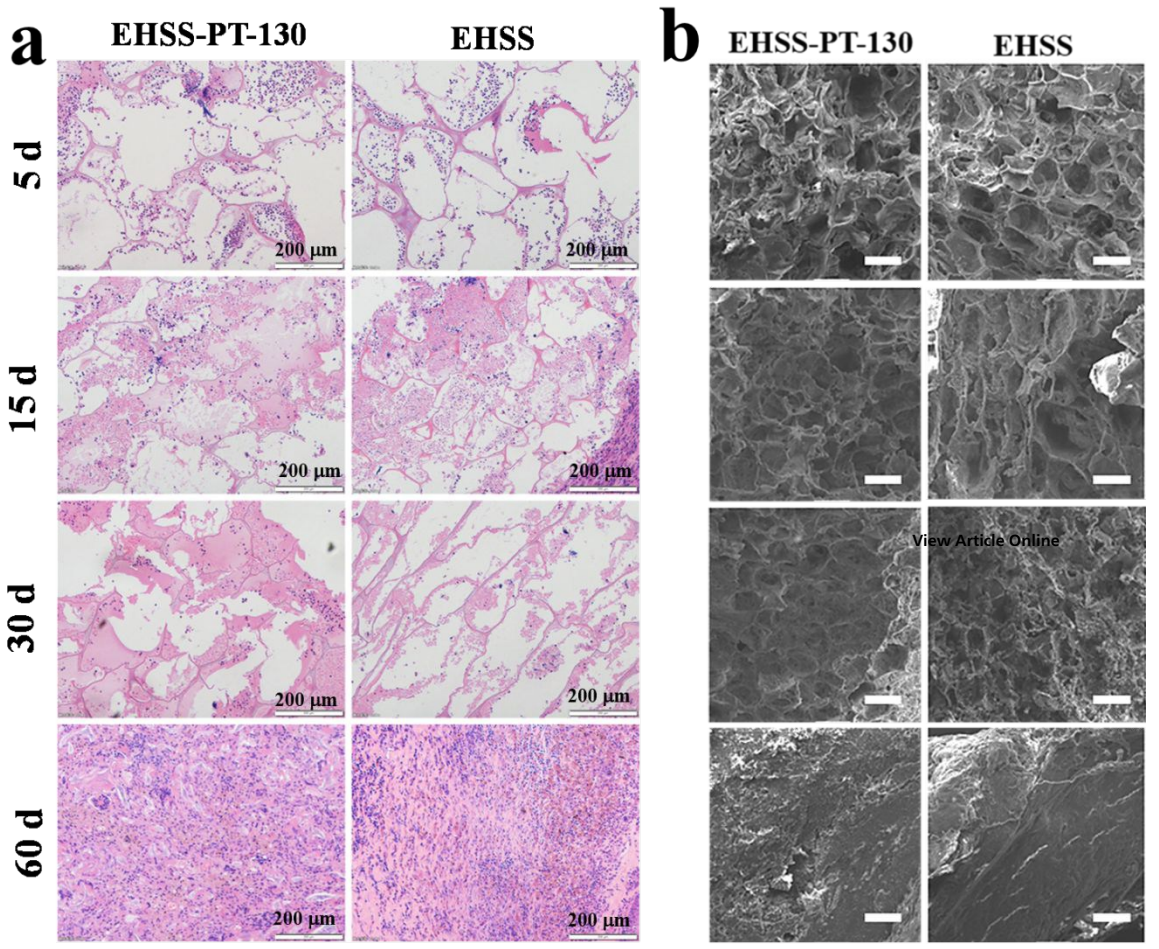

Fig. 9.

A table of contents entry

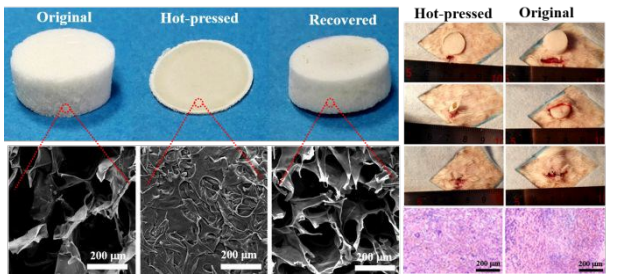

Shape memory sponges with histocompatibility and biodegradability were constructed for subcutaneous defect filling and repair, which greatly reduced surgical incision.